Acta Crystallographica Section B
Structural Science
ISSN 0108-7681

Towards direct correlations between spin-crossover and structural features in iron(II) complexes

Mathieu Marchivie,* Philippe Guionneau, Jean-François Létard and Daniel Chasseau

Institut de Chimie de la Matière Condensée de Bordeaux (ICMCB), UPR CNRS 9048, Université Bordeaux I, 87 Av. de Docteur Schweitzer, F-33608Pessac, France

Correspondence e-mail: marchivi@icmcb.u-bordeaux.fr

Received 19 March 2003
Accepted 9 May 2003

The $[Fe(PM\text{-}BiA)_2(NCS)_2]$ complex, where PM is *N*-2-pyridylmethylene and BiA is 4-aminobiphenyl, crystallizes in two polymorphs. The two phases, denoted (I) and (II), undergo a spin-crossover when the sample is cooled and present distinct spin-transition features as (I) shows a very abrupt spin transition, while (II) exhibits a gradual transition. The two forms of the complex are used to investigate the correlations that exist between the spin-transition features and structural features. This article presents the crystal structures of polymorph (II) at room temperature (high spin) and at 120 K (low spin), including a comparison with those of polymorph (I). This study reveals that the packing, in a first approximation, is similar in both forms. In order to look at the crystal structures in more detail, a new angular parameter, denoted θ_{NCS}, as well as a particular type of intermolecular hydrogen-bond interaction, which involves the S atoms of the NCS ligands, are investigated. Interestingly, this angle and this intermolecular interaction can be directly connected to the cooperativity of the spin transition. Such a result is extended to all the SCO iron(II) complexes belonging to the same family of the general formula $[Fe(PM\text{-}L)_2(NCS)_2]$.

1. Introduction

Transition metal ions in octahedral surroundings, in particular those with a $3d^4$–$3d^7$ electronic configuration, may present two electronic configurations characterized by two different spin states. Indeed, when the metal is complexed octahedrally, the ligand splits the *d* orbitals into two sets, one threefold degenerated set of orbitals, known as t_{2g}, and another twofold degenerate set of orbitals, known as e_g separated by the ligand field energy. When this ligand field energy is greater than the electron pairing energy the metal adopts the low-spin (LS) configuration where the maximum number of electrons are paired. When the ligand field energy is lower than the electron pairing energy, the metal adopts the high-spin (HS) configuration with the maximum number of uncoupled electrons. In some cases, the ligand field energy appears to be intermediate and the complex can adopt both configurations depending on external influences (temperature, pressure, light irradiation, magnetic field; Bousseksou *et al.*, 2000; Gütlich *et al.*, 1994, 2003). This phenomenon, called spin-crossover (SCO), is accompanied by a change in magnetic behaviour and can be used to obtain electronic devices (Jay *et al.*, 1993; Kahn, 1993; Kahn & Jay Martinez, 1998; O'Connor, 1996).

In the solid state the variability of the SCO features (abruptness, hysteresis, completeness *etc.*) may be, in some cases, strongly linked to the structural features. Indeed, the propagation of the spin state in a lattice, also named coop-

erativity, which can change drastically from one complex to the other (Capes *et al.*, 2000; Hauser *et al.*, 1999; Real *et al.*, 1992, 2003; Salmon *et al.*, 1999; Sugiyarto *et al.*, 2000) is suspected to be strongly connected to the crystal packing. However, this fine relation is still debated.

To contribute to the clarification of this point, we have concentrated our investigations on the iron(II) cation which can undergo a spin transition from a paramagnetic HS state, $t_{2g}^4e_g^2$ ($S = 2$), to a diamagnetic LS state $t_{2g}^6e_g^0$ ($S = 0$). In particular, we have focused on the mononuclear complex series of the general formula $[Fe(PM\text{-}L)_2(NCS)_2]$, where PM is *N*-2-pyridylmethylene and L an aromatic ligand, that have revealed very different spin-transition features (Capes *et al.*, 2000; Guionneau *et al.*, 1999; Létard *et al.*, 1998). Indeed, despite these complexes being chemically similar, their spin-transition behaviours are distinct and reveal a large range of transition temperatures ($T_{1/2}$ = 95–243 K), with strong differences in the abruptness of the transition, going from very abrupt to very gradual. Several studies on the above complexes have recently suggested that their structural features may be at the origin of the differences in their spin-crossover features (Guionneau *et al.*, 1999).

Among the complexes studied so far, $[Fe(PM\text{-}BiA)_2(NCS)_2]$, where BiA is 4-aminobiphenyl (Fig. 1), is of particular interest. It can crystallize in two distinct crystallographic phases, denoted (I) and (II). Polymorph (I) shows an extremely abrupt transition at 167 K, while polymorph (II) undergoes a gradual spin conversion centred at 205 K (Fig. 2; Létard *et al.*, 2003). Consequently, the study of this polymorphism provides a good opportunity to emphasize the role played by structural features on the spin-transitions features. It is worth noting that polymorphs of iron(II) SCO complexes have already been reported (Matouzenko *et al.*, 1997; Ozarowski *et al.*, 1988; Roux *et al.*, 1994). Nevertheless, the crystal structures of the polymorphs were not available in all the spin states. The present work represents, to our knowledge, the first comparison of the HS and LS structural features of two polymorphs in the context of a well described series of complexes.

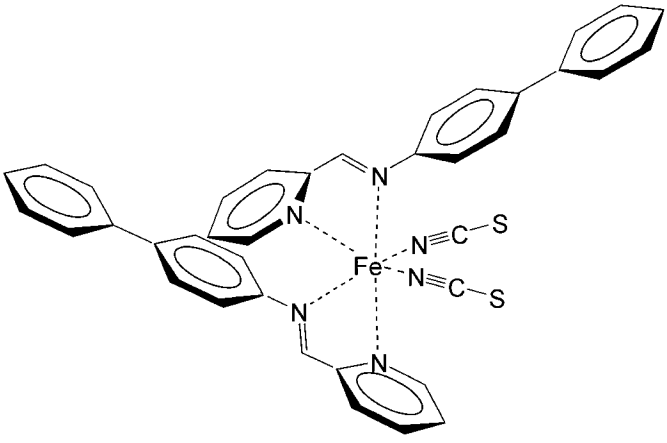

Figure 1
Scheme of the $[Fe(PM\text{-}BiA)_2(NCS)_2]$ complex.

The crystal structures of (I) in the HS and LS states have already been reported. Polymorph (I) crystallizes in an orthorhombic (*Pccn*) system. Unit-cell parameters of (II) were previously investigated by X-ray powder diffraction and a monoclinic system was suggested (Létard *et al.*, 1997, 1998). In this paper we report on the crystal structures of (II) in both spin states at 293 and 120 K. Then we compare the crystal structures of both (I) and (II) in order to identify the structural parameters responsible for the important difference in the magnetic behaviours. Finally, the observed correlations are extended to the whole $[Fe(PM\text{-}L)_2(NCS)_2]$ series.

2. Experimental

2.1. Synthesis

The PM-BiA ligand was obtained using stoichiometric amounts of 4-aminobiphenyl and carboxaldehyde-2-pyridine. These reagents were dissolved in benzene with one drop of acetic acid and stirred at reflux for 1 h. The acetic acid was then neutralized with sodium carbonate and the solution was filtered. The solvent was vaporized and a light brown powder was obtained.

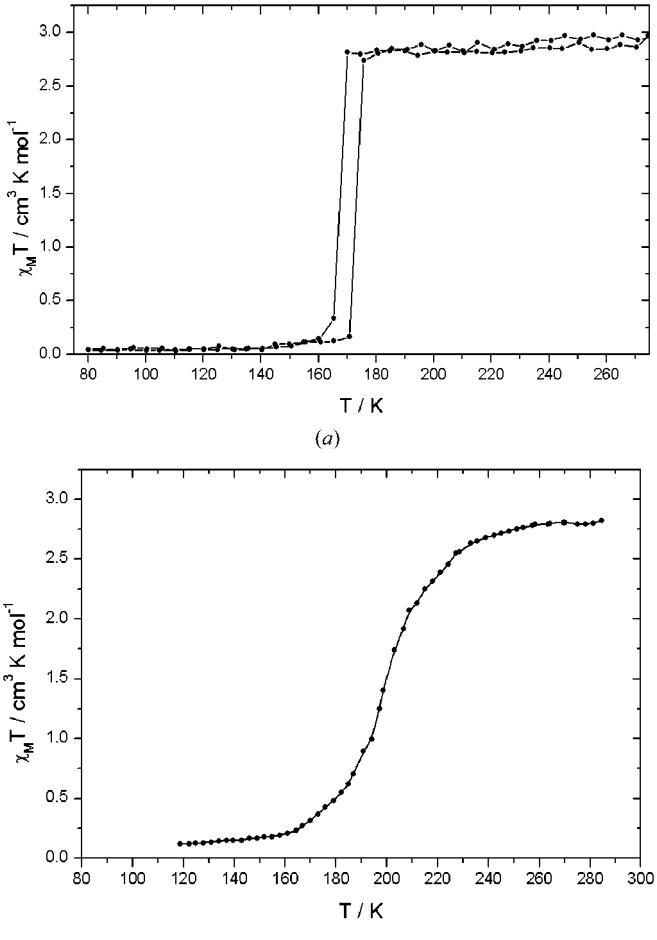

Figure 2
$\chi_M T$ product *versus* T (χ_M represents the molar magnetic susceptibility and T the temperature) in the 80–300 K range for the $[Fe(PM\text{-}BiA)_2(NCS)_2]$ polymorphs (*a*) (I) and (*b*) (II).

A small amount of this powder was dissolved in dichloromethane and placed in an H-tube containing iron thiocyanate in methanol. Black single crystals of the approximate dimensions of 0.2 × 0.3 × 0.3 mm^3 of the [Fe(PM-BiA)$_2$(NCS)$_2$] monoclinic phase were obtained after a few weeks by slow diffusion through the methanol. Note that there is not a significant difference in the morphology of polymorphs (I) and (II). However, these polymorphs are not concomitant.

2.2. X-ray diffraction

The crystallographic studies were performed using a Brucker–Nonius κ CCD diffractometer with Mo $K\alpha$ radiation. The crystals had a weak diffraction pattern. Two full sets of data were collected at two different temperatures: 293 and 120 K. An Oxford Cryosystem N_2 open-flow temperature-control system was used. The lowest temperature was achieved after cooling at a rate of 3 K min^{-1}. In both cases a full sphere was collected based on φ- and ω-scans at different κ values. Frames were collected at 50 s per degree at room temperature and at 60 s per degree at 120 K. The cell parameter determination and the integration of the diffraction frames were performed using the *COLLECT* program (Nonius, 1998) on the full set of data. The structures were solved with the *Sir*97 program (Altomare *et al.*, 1999) and refinement, based on full-matrix least-squares on F^2, was performed using the *SHELXL* program (Sheldrick, 1997). No absorption correction was needed owing to the low absorption coefficient of these complexes. Calculation of the different geometrical parameters Σ, θ, d_{Fe-N} and intemolecular distances were carried out using *PLATON* (Spek, 1990) and figures were made using *ORTEP* (Johnson, 1965; Farrugia, 1997). All the above softwares were used within the *WINGX* package (Farrugia, 1999). At 293 K H atoms were treated according to the riding model during refinement with isotropic displacement parameters, corresponding to the C atom they are linked to. At 120 K H atoms were located in Fourier maps and their positions were refined freely.

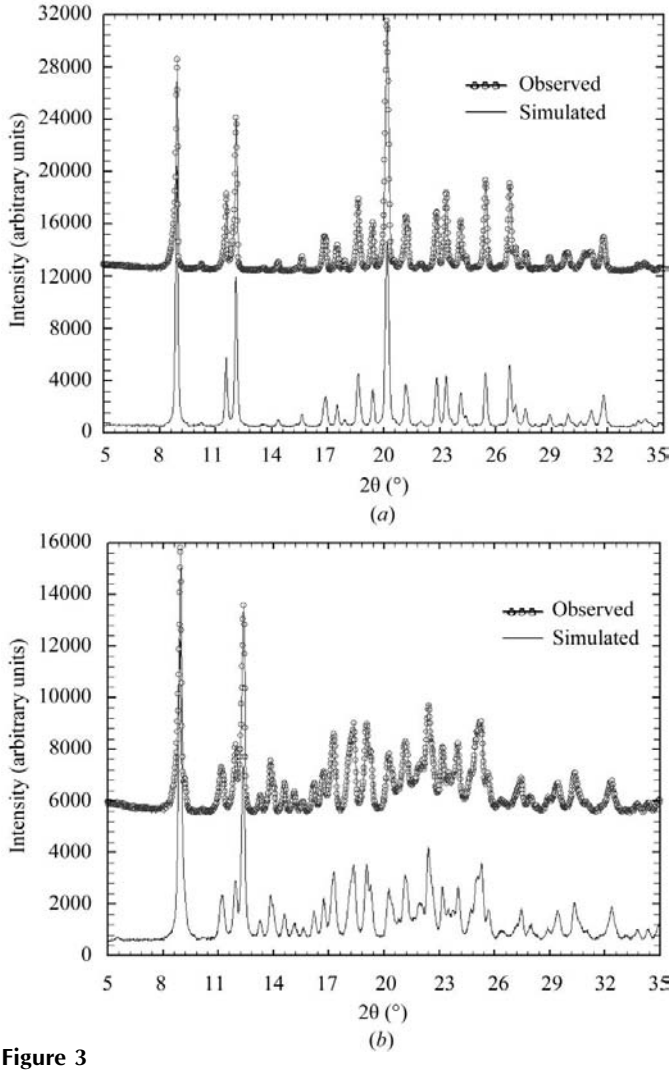

Figure 3
Experimental and simulated powder diffractograms of (*a*) polymorphs (I) and (*b*) (II) of [Fe(PM-BiA)$_2$(NCS)$_2$].

The temperature dependences of the cell parameters were measured using the same diffractometer. The cell parameters were determined every 5 K at the cooling rate of 2 K min^{-1} from 293 to 90 K. Each data set was collected using a 20° φ-scan at fixed κ (60°) in order to avoid low-temperature contractions of the goniometer head. Frames were collected at 30 s per degree.

Since single crystals were used to determine the structural features of the complexes, while magnetic measurements (SQUID magnetometer) were performed using powder samples, it was necessary to verify that the powder samples and the single crystals correspond to the same crystallographic phase. To this end, we compared the simulated powder diffractogram from the single-crystal structural data to the experimental powder diffraction data of the same sample (Fig. 3). In both cases, the latter matches the former.

X-ray powder diffraction was performed on both phases of the complex on a Philips X'pert diffractometer (Cu $K\alpha$) within the 5–50° 2θ range, using 10 s exposure times for every 0.02° step.

3. Results and discussion

3.1. Crystal structure and comparison

3.1.1. Crystal packing. In both spin states, polymorph (II) crystallizes in the monoclinic $P2_1/c$ space group. The experimental and crystallographic data are given in Table 1.[1]

One of the terminal aromatic rings presents a static disorder (Fig. 4). Such a feature is common in this series of spin-transition complexes. The asymmetric unit contains one molecule and the unit cell is therefore built on four entities. Within the *ac* plane, the neighbouring entities are symmetrical about a 2_1 screw axis and appear in an antiparallel orientation. Along the *c* direction, the adjacent complexes form a zigzag. The packing

[1] Supplementary data for this paper are available from the IUCr electronic archives (Reference: NA5001). Services for accessing these data are described at the back of the journal.

is driven by numerous π–π interactions within the *ac* plane as well as intermolecular contacts involving the NCS ligands between neighbouring complexes within the *b* direction (Fig. 5). At this point, both polymorphs of the complex studied appear to have similar packing. Besides, as both polymorphs are built on the same number of molecules in the same unit-cell volume, the monoclinic phase appears to be as compact as the orthorhombic phase. Therefore, the large differences in the SCO behaviour of the two polymorphs are not yet explained.

3.1.2. Crystallographic unit cell. A significant contraction of the unit cell occurs upon cooling from 293 to 120 K. It corresponds to a decrease of 4.9% of the unit-cell volume. This contraction is due to both thermal and spin-crossover effects. These effects can be separated using an isostructural complex of cobalt: $[Co(PM\text{-}BiA)_2(NCS)_2]$, which does not undergo any spin-crossover (Guionneau *et al.*, 2002). It is then possible to extract the contraction of the unit-cell volume due only to spin-crossover, denoted as ΔV_{SC}; in (II), ΔV_{SC} (70 Å^3) corresponds to 2% of the room-temperature unit-cell volume and the values found for all the studied complexes within the series agree precisely (1.9–2.4%; Guionneau *et al.*, 1999, 2001, 2002).

The contraction of the unit-cell parameters of the orthorhombic form of this complex shows strong anisotropy between room temperature and 140 K. Such a feature has been suspected to play an important role in the spin-transition abruptness (Guionneau *et al.*, 1999). Fig. 6 shows the evolution of the unit-cell parameters upon cooling for the monoclinic phase (II); it also reveals a strong anisotropy. Indeed, the modifications of *a*, *b* and *c* are very different at the SCO: *b* and *c* decrease by approximately 2% while *a* increases by 1%. Moreover, the temperature dependence of the cell parameters out of the spin-transition zone also presents anisotropy; *a* remains quasi-constant, *b* decreases slightly (0.6×10^{-3} Å K^{-1}) and *c* strongly decreases (3.4×10^{-3} Å K^{-1}). Surprisingly, this behaviour is similar to the temperature dependence of the first polymorph. Consequently, this feature cannot be taken into account to explain the drastic differences in the magnetic susceptibility curves. Therefore, the crystal structure must be discussed in more detail.

3.1.3. Fe—N_6 geometry. It is well known that the main structural

Table 1
Experimental data.

Orthorhombic data from Létard *et al.* (1998).

	Experimental conditions			
Parameters	Monoclinic form (II)		Orthorhombic form (I)	
Chemical formula	$FeC_{38}H_{28}N_6S_2$			
T (K)	293	120	293	140
a (Å)	17.570 (5)	17.362 (1)	12.949 (7)	12.370 (3)
b (Å)	12.602 (5)	12.362 (1)	15.183 (2)	14.764 (3)
c (Å)	17.358 (5)	17.050 (1)	17.609 (5)	18.281 (4)
β (°)	115.68 (1)	115.83 (1)	90.00	90.00
V (Å^3)	3464 (2)	3294 (1)	3462 (2)	3339 (2)
Space group	$P2_1/c$	$P2_1/c$	*Pccn*	*Pccn*
Z	4	4	8	8
Spin state	HS	LS	HS	LS
Radiation	Mo $K\alpha$	Mo $K\alpha$	Mo $K\alpha$	Mo $K\alpha$
Calculated density (g cm^{-3})	1.321	1.389	–	–
μ (mm^{-1})	0.59	0.62	–	–
Apparatus	κ CCD	κ CCD	–	–
θ range (°)	1.29–25.02	1.30–27.48	–	–
h min/max	−20/20	−22/22	–	–
k min/max	−14/14	−16/16	–	–
l min/max	−20/20	−22/22	–	–
No. of reflections measured	23166	29088	–	–
No. of independent reflections	6118	7540	–	–
No. of parameters	424	536	–	–
Criterion for observed reflections	$I > 2\sigma(I)$	$I > 2\sigma(I)$	–	–
R_{int}	0.041	0.053	–	–
R_{obs}	0.051	0.039	0.045	0.043
$wR_{obs}(F^2)$	0.144	0.103	–	–
$(\Delta/\sigma)_{max}$	0.000	0.001	–	–
$\Delta\rho$ (e Å^{-3})	0.68/−0.88	0.67/−1.02	–	–

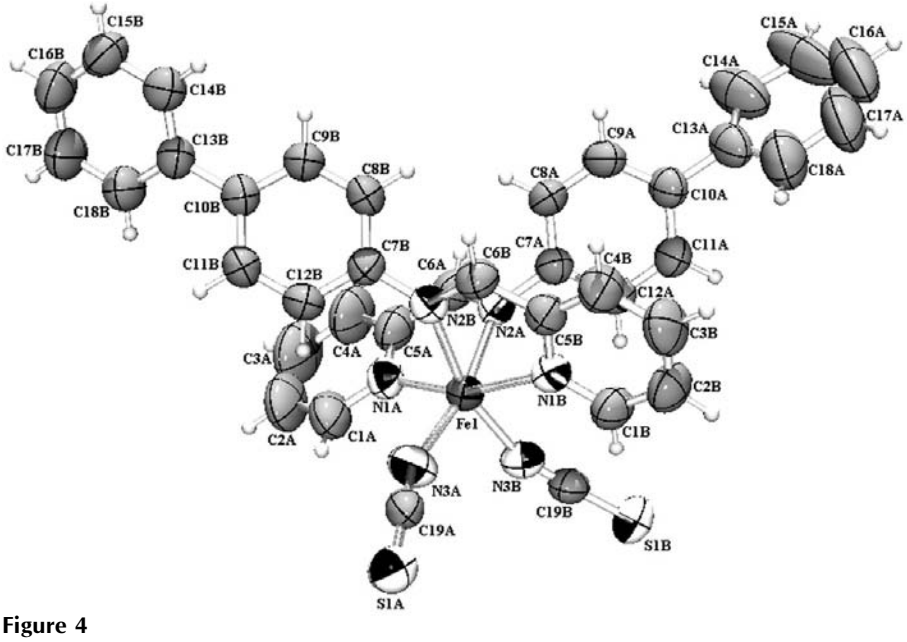

Figure 4
ORTEP (Johnson, 1965; Farrugia, 1997) view of the asymmetric unit of $[Fe(PM\text{-}BiA)_2(NCS)_2]$ in the HS form of polymorph (II) (293 K). Displacement ellipsoids are at the 50% level.

Table 2
Fe—N bond distances in $[Fe(PM\text{-}BiA)_2(NCS)_2]$, polymorph (II), in the HS state (293 K) and the LS state (120 K).

	*d*Fe—N (Å)		
Fe—N	293 K	120 K	$d_{293\ K} - d_{120\ K}$ (Å)
Fe1—N1A	2.154 (3)	1.959 (2)	0.195 (4)
Fe1—N1B	2.177 (3)	1.970 (2)	0.207 (4)
Fe1—N2A	2.250 (4)	1.965 (3)	0.285 (5)
Fe1—N2B	2.241 (2)	1.969 (2)	0.272 (3)
Fe1—N3A	2.065 (5)	1.948 (3)	0.117 (6)
Fe1—N3B	2.076 (3)	1.950 (2)	0.126 (4)

modifications at the spin-crossover concern the iron coordination sphere (Guionneau *et al.*, 1999; Gütlich, 1981; König, 1987; König & Madeja, 1966; Konno & Mikami-kido, 1991; Moliner *et al.*, 1999; Takemoto & Hutchinson, 1973). The expansion (LS to HS transition) or contraction (HS to LS transition) of the coordination sphere and the distortion of the $Fe—N_6$ octahedron can be probed by different parameters such as the mean iron–nitrogen distances, $\langle d_{Fe\text{-}N}\rangle$, and the Σ parameter, which represents the sum of the deviation from 90° of the 12 *cis* angles in the coordination sphere of the Fe atom and thus reflect the deformation of the octahedron. These two parameters are known to depend only on the spin state (Guionneau *et al.*, 2001, 2002).

When (II) undergoes the spin transition from the HS to the LS state, the iron–nitrogen distances decrease and become more homogeneous. The Fe—N distances range from 2.066 (4) to 2.250 (4) Å in the HS state and from 1.948 (2) to 1.970 (2) Å in the LS state (Table 2). In addition, the $Fe—N_6$ octahedron becomes more regular. Table 3 collects the values of the intramolecular parameters $\langle d_{Fe—N}\rangle$ and Σ. They clearly indicate that (II) is in the HS state at room temperature and in the LS state at 120 K. Indeed, these parameters lie in the range observed for all the other complexes of this series: $\Sigma \simeq 80°$, $\langle d_{Fe\text{-}N}\rangle \simeq 2.14$ Å for the HS state with Σ around 45° and $\langle d_{Fe—N}\rangle$ around 1.95 Å in the LS state. Moreover, it is interesting to note that both (I) and (II) give similar $\langle d_{Fe—N}\rangle$ and Σ values despite exhibiting opposite magnetic behaviour. Such a result proves, once more, that these parameters are characteristic only of the spin state and not of the spin-transition features (Guionneau *et al.*, 2003). This remark, in fact, is not so surprising as the spin-transition features depend more on the cooperativity factor linked to the intermolecular interactions

Table 3
Geometry of the $Fe—N_6$ octahedron for polymorphs (I) and (II) of $[Fe(PM\text{-}BiA)_2(NCS)_2]$ (see text for definitions).

	$[Fe(PM\text{-}BiA)_2(NCS)_2]$, I		$[Fe(PM\text{-}BiA)_2(NCS)_2]$, II	
T (K)	293	140	293	120
Spin state	HS	LS	HS	LS
⟨*d*Fe—N(CS)⟩ (Å)	2.041 (8)	1.939 (2)	2.071 (4)	1.949 (2)
⟨*d*Fe—N(PM)⟩ (Å)	2.241 (8)	1.965 (2)	2.205 (4)	1.966 (2)
Σ (°)	86 (2)	48 (2)	80 (2)	43 (2)

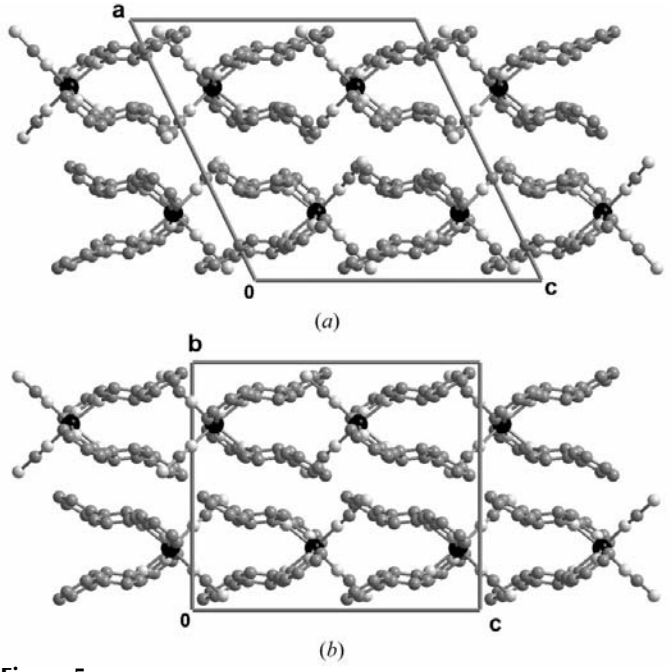

Figure 5
View of the packing of $[Fe(PM\text{-}BiA)_2(NCS)_2]$, (*a*) form (II) along the *b* axis and (*b*) form (I) along the *a* axis. H atoms are omitted for clarity.

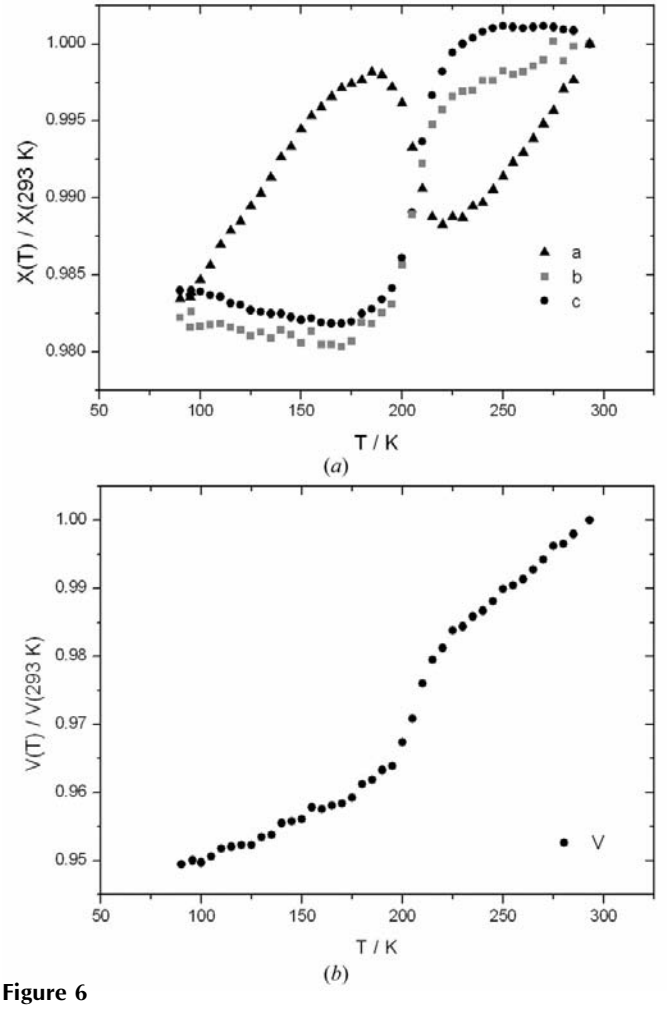

Figure 6
Relative temperature dependence of (*a*) the unit-cell parameters and (*b*) the unit-cell volume for $[Fe(PM\text{-}BiA)_2(NCS)_2]$, polymorph (II). Standard deviations: $\sigma < 0.005$ Å (0.04%) for *a*, *b* and *c*, and $\sigma < 2$ Å^3 (0.06%) for the unit-cell volume.

Table 4
θ_{NCS} and S···H(C) distance values for the $[Fe(PM\text{-}L)_2(NCS)_2]$ series .

A = 4-(thienylethynyl)aniline, PEA = 4-(phenylethynyl)aniline, AzA = 4-(phenylazo)aniline and TEA = 4-aminoterphenyl.

$[Fe(PM\text{-}L)_2(NCS)_2]$	Label	θ_{NCS} (HS) (°)	θ_{NCS} (LS) (°)	S···C(H) distance (Å), 293 K
$[Fe(PM\text{-}BiA)_2(NCS)_2]$, (I)	1	30 (1)	45 (1)	3.41 (1)
$[Fe(PM\text{-}BiA)_2(NCS)_2]$, (II)	2	37 (1)	47 (1)	3.54 (1)
m-$[Fe(PM\text{-}TheA)_2(NCS)_2]$	3	35 (1)	43 (1)	3.47 (1)
o-$[Fe(PM\text{-}TheA)_2(NCS)_2]$	4	–†	43 (1)	3.53 (1)
$[Fe(PM\text{-}PEA)_2(NCS)_2]$	5	35 (1)	43 (1)	3.46 (1)
$[Fe(PM\text{-}AZA)_2(NCS)_2]$	6	37 (1)	45 (1)	3.49 (1)
$[Fe(PM\text{-}TEA)_2(NCS)_2]$	7	39 (1)	43 (1)	3.60 (1)

† Not totally HS at room temperature.

Table 5
Geometric data concerning the C—H···S interaction for $[Fe(PM\text{-}BiA)_2(NCS)_2]$, polymorph (II), at 293 K (HS) and 120 K (LS).

T (K)	C—H···S	C—H (Å)	H···S (Å)	C···S (Å)	C—H···S (°)
293	C11*A*—H11*A*···S1*B*	0.93 (1)	2.87 (1)	3.54 (1)	130.3 (2)
120	C11*A*—H11*A*···S1*B*	0.95 (1)	2.75 (1)	3.45 (1)	131.0 (2)

than on the intramolecular modification of the iron coordination sphere. Therefore, other structural parameters have to be considered to account for the particular spin-transition features of both phases of this complex.

3.2. Structural parameters *versus* cooperativity

3.2.1. θ_{NCS} parameter *versus* SCO features. In addition to using the above intramolecular parameters to characterize the Fe—N_6 octahedron, we have investigated a new parameter, θ_{NCS}, which takes into account the variation in bond lengths together with the distortion of the octahedron.

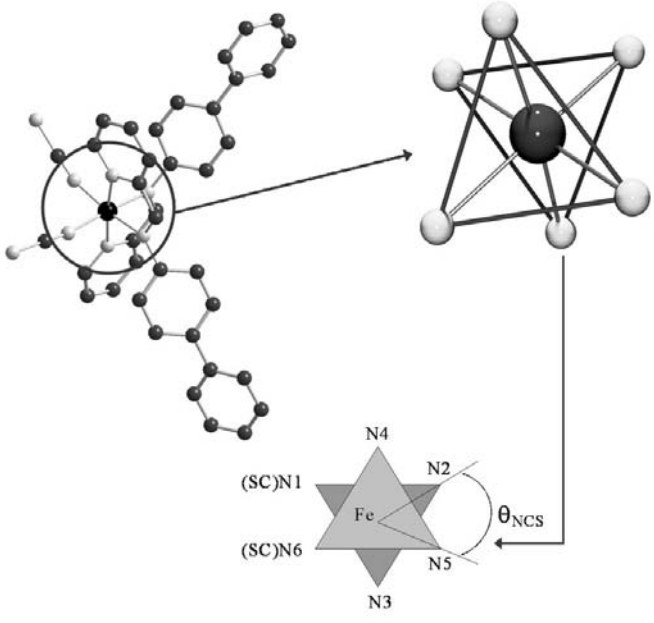

Figure 7
Definition of the intramolecular angle θ_{NCS} used to characterize both the expansion and the deformation of the Fe—N_6 octahedron at the spin-crossover.

The parameter θ_{NCS} is derived from the twist angle of an octahedral geometry (Drew *et al.*, 1995; Létard, *et al.*, 1998; McCusker *et al.*, 1996; Musher, 1972; Purcell, 1979) and is defined as follows. The Fe—N_6 octahedron of the complex always viewed along the same direction is projected onto a plane perpendicular to one of its threefold axes. The investigated angle, θ_{NCS}, is the N—Fe—N angle which is opposite the NCS ligands (Fig. 7). According to this definition, θ_{NCS} must be equal to 60° in an ideal octahedron. Therefore, deviations from 60° show octahedral distortion. Conversely to Σ, which characterizes the global octahedral distortion, θ_{NCS} characterizes a specific distortion linked to the NCS ligands and to the aromatic ligands. This angle is thereby connected to the intermolecular interactions which principally involve the NCS ligands and the aromatic ligands.

In order to elaborate further on this point it is necessary to give a definition of the numerical value of the spin-transition abruptness chosen here to represent the cooperative nature of the system: the abruptness of the transition is represented by the temperature gap, denoted as Δa, which is needed for a given complex to undergo a thermal spin transition from 80% HS to 80% LS. This naïve definition implies that the larger the Δa value the smoother the transition.

Table 4 provides the θ_{NCS} values for the $[Fe(PM\text{-}L)_2(NCS)_2]$ series. Low θ_{NCS} angles indicate a noticeable distortion of the octahedron corresponding to a HS state, while θ_{NCS} angles closer to 60° indicate a LS state.

A close examination of the HS state θ_{NCS} values for both phases of $[Fe(PM\text{-}BiA)_2(NCS)_2]$ reveals a significant difference between the orthorhombic (θ_{NCS} = 30°) and the monoclinic (θ_{NCS} = 37°) forms. Fig. 8 shows the evolution of the θ_{NCS} angle *versus* Δa, as defined above, for all the known complexes of this family. This angle is also spin-state dependent, therefore, all the complexes studied here are taken when they are 100% in the HS state. The shape of the curve obtained in this way clearly indicates that θ_{NCS} is related to the abruptness of the transition. This confirms the assumption that θ_{NCS}, in addition to being a spin-state characteristic, depends on the spin-transition features and consequently on the cooperativity of the system. Note that to our knowledge it is the first time that a direct correlation between one intramolecular parameter and the SCO cooperative behaviour is shown. Such a characteristic of θ_{NCS} can be understood if we consider that the definition of this angle is strongly dependent on the NCS ligands and aromatic ligands.

3.2.2. S···H—C hydrogen bonds. Another approach to understanding the difference in spin-transition features is to examine the intermolecular interactions. Previous studies have shown that, in general, π stacking is connected to the

cooperativity of the spin transition and to the presence or absence of a hysteresis loop (Gütlich, 1981; Gütlich *et al.*, 1996; König, 1987). Nevertheless, the π–π interaction network appears to be similar in both polymorphs of [Fe(PM-BiA)$_2$(NCS)$_2$] and consequently cannot account for differences in SCO abruptness. According to this remark we have investigated the intermolecular hydrogen contacts S···H—C involving the S atoms of the NCS ligands (Fig. 9). Table 5 gathers the detailed data concerning this interaction for polymorph (II).

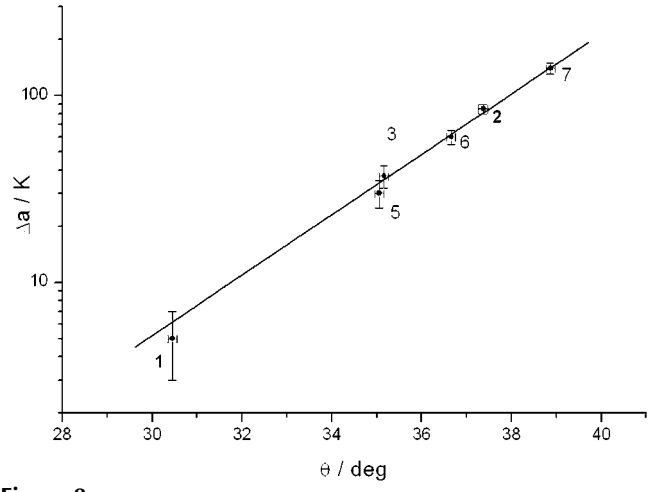

Figure 8
Δa evolution *versus* θ_{NCS} angle (see text for definition). See Table 3 for the corresponding numbers.

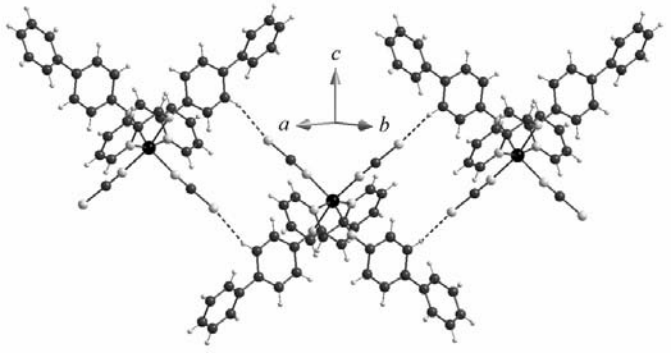

Figure 9
View of the intermolecular hydrogen S···H—C bonds in the [Fe(PM-L)$_2$(NCS)$_2$] series discussed in this paper. L = BiA is the example.

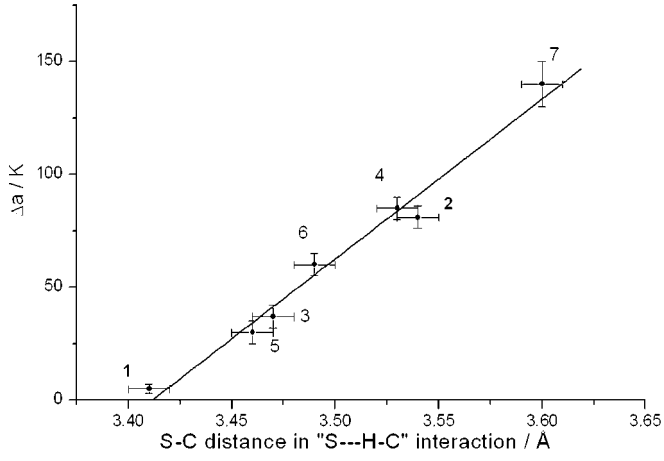

Figure 10
Evolution of Δa (defined in the text) *versus* the shortest intermolecular sulfur–carbon distance involved in the S···H—C hydrogen interaction.

This contact seems to be the main difference in the intermolecular interaction network between polymorphs (I) and (II). As the H atoms had to be treated geometrically, the S···C(H) distances should rather be used than the corresponding S···H(C) distances to define this interaction. Table 4 shows the large distribution of this distance within the [Fe(PM-L)$_2$(NCS)$_2$] family. It appears, for instance, significantly longer in (II) than in (I).

Fig. 10 presents a plot of the Δa value *versus* the distance previously defined among the complexes of the studied series. The correlation between the abruptness and the sulfur–carbon contact is therefore proved by the linear variation of Δa as a function of the S···C intermolecular contact. In particular, the difference in this distance perfectly matches the gap in abruptness for the [Fe(PM-BiA)$_2$(NCS)$_2$] polymorphs, but also for the monoclinic and the orthorhombic polymorphs of [Fe(PM-TheA)$_2$(NCS)$_2$] (Marchivie *et al.*, 2003). Such a correlation also provides proof that the variation in SCO features can be induced by small differences in the crystal packing and, in particular, by weak interactions.

Elsewhere, the photomagnetic features of the two polymorphs also show differences (Létard *et al.*, 2003). It is now established that the photomagnetic response and the thermal SCO properties ($T_{1/2}$) are directly linked (Marcen *et al.*, 2002). Consequently, the structural parameters used here to account for the thermal SCO features of the [Fe(PM-L)$_2$(NCS)$_2$] complexes might also account for the differences in the photomagnetic properties.

4. Conclusions

The study of the two polymorphs of [Fe(PM-BiA)$_2$(NCS)$_2$] firstly reveals the similar structural features for the two forms. In order to extract the relevant structural differences, a new intramolecular parameter, θ_{NCS}, and the S···H—C intermolecular hydrogen bonds have been investigated. Then, both structural features have been directly correlated to the difference of the abruptness of the spin transition, this correlation being extended to all the [Fe(PM-L)$_2$(NCS)$_2$] SCO complexes.

Such a direct correlation proves the relationship between the structural parameters, both intra- or intermolecular, and the SCO abruptness. Moreover, this study also shows that weak intermolecular interactions can strongly influence the SCO features. Such a result is of crucial importance in the context of the design of new SCO materials that must fulfil the requirements for practical applications (Kahn *et al.*, 1992).

References

Altomare, A., Burla, M. C., Camalli, M., Cascarano, C., Giacovazzo, C., Guagliardi, A., Moliterni, A. G. G., Polidori, G. & Spagna, R. (1999). *J. Appl. Cryst.* **32**, 115–119.

Bousseksou, A., Negre, N., Salmon, L., Tuchagues, J.-P., Boillot, M.-L., Boukheddaden, K. & Varret, F. (2000). *Eur. Phys. J. B*, **13**, 451–456.

Capes, L., Létard, J.-F. & Kahn, O. (2000). *Chem. Eur. J.* **6**, 2246–2255.

Drew, M. G. B., Harding, C. J., McKee, V., Morgan, G. G. & Nelson, J. (1995). *J. Chem. Soc. Chem. Commun.* pp. 1035–1038.

Farrugia, L. J. (1997). *J. Appl. Cryst.* **30**, 565.

Farrugia, L. J. (1999). *J. Appl. Cryst.* **32**, 837–838.

Guionneau, P., Brigouleix, C., Barrans, Y., Goeta, A. E., Létard, J.-F., Howard, J. A. K., Gaultier, J. & Chasseau, D. (2001). *C. R. Acad. Sci. Ser. IIc*, **4**, 161–171.

Guionneau, P., Létard, J.-F., Yufit, D. S., Chasseau, D., Bravic, G., Goeta, A. E., Howard, J. A. K. & Kahn, O. (1999). *J. Mater. Chem.* **9**, 985–994.

Guionneau, P., Marchivie, M., Bravic, G., Létard, J.-F. & Chasseau, D. (2002). *J. Mater. Chem.* **12**, 2546–2551.

Guionneau, P., Marchivie, M., Bravic, G., Létard, J.-F. & Chasseau, D. (2003). *Top. Curr. Chem.* In the press.

Gütlich, P. (1981). *Struct. Bonding*, **44**, 83.

Gütlich, P., Garcia, Y. & Spiering, H. (2003). *Magnetism: Molecules to Materials IV*, edited by J. S. Miller. New York: Wiley-CH.

Gütlich, P., Hauser, A. & Spiering, H. (1994). *Angew. Chem. Int. Ed.* **33**, 2024.

Gütlich, P., Jung, J. & Goodwin, H. A. (1996). *Molecular Magnetism: from Molecular Assemblies to the Devices, NATO ASI*, edited by E. Coronado, P. Delhaes, D. Gatteschi and J. S. Miller, Vol. E321, p. 27. Dordrcht: Kluwer.

Hauser, A., Jeftic, J., Romstedt, H., Hinek, R. & Spiering, H. (1999). *Coord. Chem. Rev.* pp. 471–491.

Jay, C., Grolière, F., Kahn, O. & Kröber, J. (1993). *Mol. Cryst. Liq. Cryst. A*, **324**, 255.

Johnson, C. K. (1965). Report ORNL-3794. Oak Ridge National Laboratory, Tennessee, USA.

Kahn, O. (1993). *Molecular Magnetism.* New York: VCH.

Kahn, O. & Jay Martinez, C. (1998). *Science*, **279**, 44–48.

Kahn, O., Kröber, J. & Jay, C. (1992). *Adv. Mater.* **4**, 718.

König, E. (1987). *Prog. Inorg. Chem.* **35**, 527.

König, E. & Madeja, K. (1966). *J. Chem. Soc. Chem. Commun.* pp. 61–62.

Konno, M. & Mikami-kido, M. (1991). *Bull. Chem. Soc. Jpn*, **64**, 339–345.

Létard, J.-F., Chastanet, G., Nguyen, O., Marcen, S., Marchivie, M., Guionneau, P., Chasseau, D. & Gütlich, P. (2003). *Monatsh. Chem.* **134**, 165–182.

Létard, J.-F., Guionneau, P., Rabardel, L., Howard, J. A. K., Goeta, A. E., Chasseau, D. & Kahn, O. (1998). *Inorg. Chem.* **37**, 4432–4441.

Létard, J.-F., Montant, S., Guionneau, P., Martin, P., Le Calvez, A., Freysz, E., Chasseau, D., Lapouyade, R. & Kahn, O. (1997). *J. Chem. Soc. Chem. Commun.* **8**, 745–746.

Marcen, S., Lecren, L., Capes, L., Goodwin, H. A. & Létard, J.-F. (2002). *Chem. Phys. Lett.* **358**, 87–95.

Marchivie, M., Kollmannsberger, M., Guionneau, P., Létard, J.-F. & Chasseau, D. (2003). To be published.

Matouzenko, G. S., Bousseksou, A., Lecocq, S., Koningsbruggen, P. J. v., Perrin, M., Kahn, O. & Collet, A. (1997). *Inorg. Chem.* **36**, 5869–5879.

McCusker, J. K., Rheingold, A. L. & Hendrickson, D. N. (1996). *Inorg. Chem.* **35**, 2100–2112.

Moliner, N., Muñoz, M. C., Létard, S., Létard, J.-F., Solans, X., Burriel, R., Castro, M., Kahn, O. & Real, J.-A. (1999). *Inorg. Chem. Acta*, **291**, 279–288.

Musher, J. I. (1972). *Inorg. Chem.* **11**, 2335–2340.

Nonius. (1998). *Collect.* Nonius BV, Delft, The Netherlands.

O'Connor, C. J. (1996). *Molecular Magnetism: from Molecular Assemblies to the Devices, NATO ASI*, edited by E. Coronado, P. Delhaes, D. Gatteschi and J. S. Miller, Vol. E321, p. 521. Dordrecht: Kluwer.

Ozarowski, A., McGarvey, B. R., Sarkar, A. B. & Drake, J. E. (1988). *Inorg. Chem.* **27**, 628–635.

Purcell, K. F. (1979). *J. Am. Chem. Soc.* **101**, 5147–5152.

Real, J.-A., Gallois, B., Granier, T., Suez-Panama, F. & Zarembowitch, J. (1992). *Inorg. Chem.* **31**, 4972–4979.

Real, J.-A., Gaspar, A. B., Niel, V. & Muñoz, M. C. (2003). *Coord. Chem. Rev.* **236**, 121–141.

Roux, C., Zarembowitch, J., Gallois, B., Garnier, T. & Claude, R. (1994). *Inorg. Chem.* **33**, 2273–2279.

Salmon, L., Donnadieu, B., Bousseksou, A. & Tuchagues, J.-P. (1999). *C. R. Acad. Sci. Ser. IIc*, **2**, 305–309.

Sheldrick, G. M. (1997). *SHELX*97. University of Göttingen, Germany.

Spek, A. L. (1990). *Acta Cryst.* A**46**, C34.

Sugiyarto, K. H., Scudder, M. L., Craig, D. C. & Goodwin, H. A. (2000). *Aust. J. Chem.* **53**, 755–765.

Takemoto, J. H. & Hutchinson, B. (1973). *Inorg. Chem.* **12**, 705–708.